Proc. Natl. Acad. Sci. USA
Vol. 87, pp. 8311–8315, November 1990
Biophysics

Gating current associated with inactivated states of the squid axon sodium channel

(inactivation/voltage clamp/kinetic model)

J. M. BEKKERS*†‡, I. C. FORSTER*§, AND N. G. GREEFF*§

*Station Marine de Roscoff, 29211 Roscoff, France; †The Salk Institute, Howard Hughes Medical Institute, 10010 North Torrey Pines Road, La Jolla, CA 92037; and §Physiologisches Institut, Universität Zürich-Irchel, Winterthurerstrasse 190, 8057 Zürich, Switzerland

Communicated by Charles F. Stevens, August 2, 1990

ABSTRACT **Sodium (Na) channel gating currents were measured in squid (*Loligo forbesi*) axons to study transitions among states occupied by the Na channel when it is inactivated. These measurements were made at high temporal resolution with a low-noise voltage clamp. The inactivation-resistant gating current, $I_{g,inact}$, could be separated into a very fast (τ = 5–25 μs) and a slower (τ = 40–200 μs) component over a wide range of test potentials (−140 mV to 80 mV) and for three different starting potentials (−70 mV, 0 mV, and 50 mV). The time constants for these components plotted against test potential lay on two bell-shaped curves; the time constants at any particular test potential did not depend on the starting potential. Both components had charge–voltage curves that saturated between −150 mV and 50 mV. A fast spike, similar to the fast component of $I_{g,inact}$, was also apparent in recordings of the fully recovered total "on" gating current. $I_{g,inact}$ (fast) and $I_{g,inact}$ (slow) could not together be described by the simplest possible model, a linear three-state scheme; however, $I_{g,inact}$ (fast) could be modeled by a two-state scheme operating in parallel with other gating processes. $I_{g,inact}$ (slow) and the gating current due to recovery from inactivated states into resting states could together be well described by a three-state scheme. This lends support to models in which a pair of inactivated states are connected by a single voltage-dependent step to the resting states of the Na system.**

The Na channel in the squid axon is known to have a complex kinetic structure with perhaps several resting states (1), two or three open states (2, 3), and two or more inactivated states (4, 5). Many attempts have been made to devise models that account for all possible states of the channel (e.g., refs. 3 and 6), but these often prove difficult to quantify because of the many adjustable parameters. Our approach was to confine the study to a manageable subset of the states that could be studied in detail; the resultant model might then be fitted into a larger scheme. The inactivated states of the Na channel were chosen because (*i*) they are operationally well defined (entered by applying an inactivating prepulse), (*ii*) they are kinetically isolated because recovery from them into resting states happens relatively slowly, and (*iii*) the form of the gating current associated with them is known to be simple (1), although the kinetics of this gating current has not been analyzed in detail.

During our experiments we observed another, very fast component in the gating current; this component could only be observed in fresh axons, for which the membrane could be rapidly voltage clamped. The very fast component appeared independent of the inactivation state of the Na channel and was adequately modeled as a two-state scheme functioning in parallel with other gating processes. On the other hand, the previously described slow component of the inactivation-resistant gating current (1) was well-modeled as a two-state scheme connected via a single voltage-dependent step to the resting states of the Na channel. This scheme can be regarded under specific conditions as a subset of general schemes like those of Armstrong and Bezanilla (3) and Armstrong and Gilly (1).

These results were obtained by using a recently designed low-noise voltage clamp system that assisted us in making higher-resolution measurements than were hitherto possible.

MATERIALS AND METHODS

Axons from freshly killed squid (*Loligo forbesi*) were internally dialyzed as described (7) and voltage clamped at 5°C in an air-gap chamber. Other details were as follows.

Data Acquisition. Membrane currents were filtered at 100 kHz (6-pole Bessel filter) and usually sampled at 3- or 5-μs intervals. In a few experiments a transient recorder sampling at 0.5-μs intervals was used to confirm the fits found with the slower sampling. The membrane holding potential was −70 mV. Linear currents were subtracted on-line by using a scaled back-reference pulse (8) between −150 and −180 mV, where no nonlinear charge transfer occurs. Membrane capacity transients were monitored throughout each experiment by using the transient recorder.

Solutions. The external solution was 11 mM $CaCl_2$/55 mM $MgCl_2$/524 mM Tris chloride/1 μM tetrodotoxin (1155 mOsm). The internal solution was 350 mM tetramethylammonium fluoride/400 mM sucrose/10 mM Hepes (1350 mOsm). The pH of all solutions was adjusted to 7.2 at 5°C.

Voltage Clamp. Our ability to resolve a very rapid component of gating current was assisted by our use of a recently designed fast low-noise voltage clamp (see ref. 9 for details). This technique was important because experiments had to be done quickly to avoid fatigue of the fiber and obliteration of the rapid component (see *Results*); the low-noise clamp reduced the need for time-consuming signal averaging.

Much effort was expended on tuning the clamp and associated electronics for optimum noise, speed, and linearity. The total noise of the clamp plus signal conditioning hardware improved signal-to-noise ratio >10-fold compared to previous clamp designs (e.g., ref. 7), with a corresponding 100-fold reduction in signal averaging. When series resistance compensation was set for critical damping (7) and after compromising with instrumentation asymmetry (see below), the 10–90% settling time in the membrane for a command step was 8 μs. (Note that the capacity transient shown in Fig. 1*A* appears slower than this because it was filtered at 100 kHz.)

The publication costs of this article were defrayed in part by page charge payment. This article must therefore be hereby marked "*advertisement*" in accordance with 18 U.S.C. §1734 solely to indicate this fact.

Abbreviations: V_p, voltage clamp test potential; τ, time constant of exponential decay; e, charge on electron; $I_{g,inact}$, inactivation-resistant gating current; $I_{g,ON}$, fully recovered total "on" gating current.

‡To whom reprint requests should be addressed at: The Salk Institute, 10010 North Torrey Pines Road, La Jolla, CA 92037.

The linearity and symmetry of all components between the axon and the computer were studied by using a dummy circuit, comprising passive elements, to model the membrane and recording chamber. After optimization, there remained only a small, brief asymmetry (e.g., Fig. 1*B*). Only for some voltage protocols, when the gating current was very small, was the accuracy of curve fits to the data affected (see *Results*).

Curve Fitting. Gating currents were adjusted to the baseline at the end of the prepulse, and least-squares fits were performed. Records were fitted to a sum of two or (at strongly negative test potentials) three exponentials, plus a small offset at negative potentials. Sometimes the time constant of the slowest exponential was constrained (see below).

RESULTS

Clamp Speed as Determined from Capacity Transients. Because an objective was to resolve very fast components of gating current, it was important to know just how rapidly the membrane could be stepped to the voltage clamp test potential (V_p). This was routinely determined for each fiber before and after a gating current run by measuring the membrane capacity transient (I_c), which gives the rate at which the membrane is charged to V_p. Fig. 1 shows some typical results for a voltage-clamped axon with series resistance (R_s) compensation critically adjusted (7). Fig. 1*A* shows the capacity transient, measured a few minutes after mounting the fiber (trace a) and its time integral (trace b), which traces the approach of membrane potential to V_p. Fig. 1*B* shows a gating current (I_g) measured shortly afterward in this fiber by using the pulse protocol given in the Fig. 1 legend.

The capacity transient consists of a fast spike that is over in ≈15 μs, followed by a slow tail ($\tau \approx 30$ μs; arrow) that becomes more prominent the longer the axon remains in the chamber ("fatigue"; refs. 7 and 10). This tail cannot be removed by R_s compensation: increasing the compensation causes a damped oscillation about the tail, leading to an oscillatory distortion in I_g (7, 11). The effect of the slow tail is to decrease the speed of voltage clamp of the membrane (trace b), leading to distortion of fast components of I_g (for example, visible in Fig. 1*B* above the smooth curve, which is a single exponential fitted to the slower phase of I_g; see below).

An attempt was made to reduce the size of the slow component of I_c by changing osmolarities of the solutions, but this approach was unsuccessful (*cf.* ref. 12). Thus, our strategy was to start with very fresh axons and complete all critical measurements of I_g within 20–30 min.

Two or Three Components of I_g Can Be Distinguished When the Na System Is Inactivated. Fig. 2 *Insets* show three different ways of isolating the gating current that flows when the Na channel undergoes transitions between its inactivated states $I_{g,inact}$. In each case a long (20 ms) depolarizing prepulse (either to 0 mV or 50 mV) is used to inactivate the Na system. The membrane voltage is then either stepped immediately to a range of test levels (only −100, −20, and 60 mV are illustrated) or else returned briefly (0.5 ms) to −70 mV before stepping to the test levels. A gap of 0.5 ms was long enough for inactivated states to mostly attain the equilibrium distribution for the new potential but not so long that significant recovery from inactivation could occur (13). These protocols were chosen because they yield a gating current that is predominantly $I_{g,inact}$ at a range of test potentials reached from three widely spaced starting potentials (−70, 0, and 50 mV).

Two previously described components are apparent in the gating current records in Fig. 2. (*i*) At the test potential of −100 mV, Na channels recover rapidly enough from inactivation to give rise to a slow component in the gating current (3), visible as an inward plateau on this expanded time scale. (*ii*) The predominant faster component that is seen at each V_p has been qualitatively described elsewhere and is thought to arise from transitions among inactivated states of the Na channel (3). We have now observed a third, very fast component of this gating current. The superimposed dotted lines

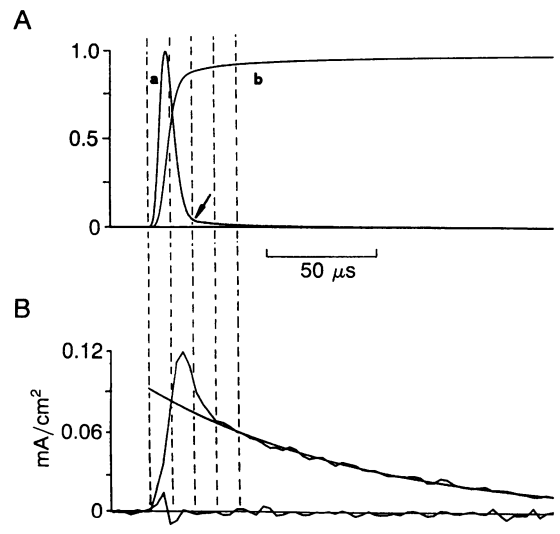

FIG. 1. The speed of voltage clamp at the membrane is limited, as revealed by the capacity transient. (*A*) Typical membrane capacity transient for a freshly mounted axon with critical series resistance (R_s) compensation (trace a) and its time integral (trace b), both normalized for clarity. Arrow, slow tail in the transient. (*B*) Gating current recorded from the same axon for a command step from −100 mV to 40 mV preceded by a 20-ms prepulse to 0 mV and a 0.5-ms gap. Smooth curve is a single exponential fit. Baseline trace is the system asymmetry recorded for the same protocol by using a passive dummy membrane. Vertical lines are 10-μs apart and indicate isochronicity. All traces were filtered with a 6-pole Bessel filter at 100 kHz.

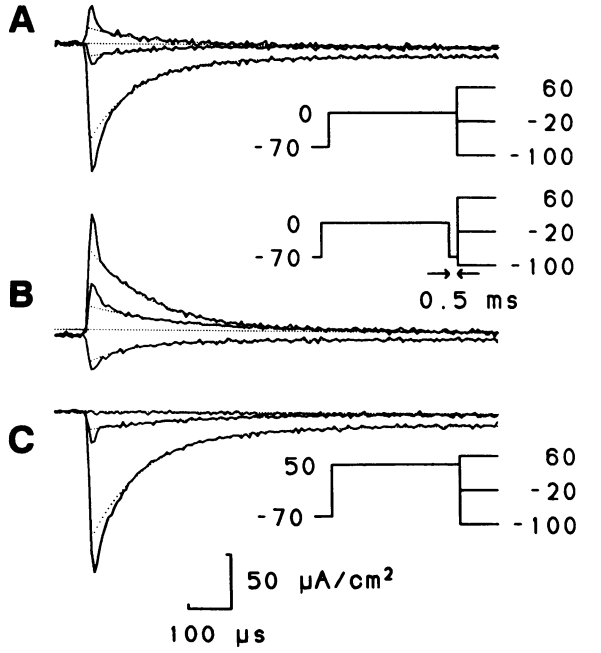

FIG. 2. (*A–C*) Inactivation-resistant gating currents, measured using the three pulse paradigms (*Insets*), possess a very fast component. Dotted curves indicate single exponential fits, except for the currents at $V_p = -100$ mV (largest negative-going current in each panel), where the curves are double-exponential fits. Each trace is an average of four sweeps.

in Fig. 2 are single exponential fits, except at $V_p = -100$ mV, where a second exponential has been added to fit the slow, recovery component. This third, very fast component is especially obvious at $V_p = -20$ and 60 mV, less so at $V_p = -100$ mV, but two exponentials (plus a third for recovery at strongly hyperpolarized V_p values) were found necessary—and to provide an excellent fit—over the whole range of test potentials used here (−140 mV to 80 mV). We do not think that this very fast component (time constant 5–20 μs) is an artifact because it cannot be accounted for by instrument asymmetry (*Materials and Methods*) or imperfect R_s compensation (14) and because the same component has been seen by us with a different voltage-clamp system (7, 11). Furthermore, a similar component is visible in the records of Alicata *et al.* (15), obtained in crayfish axons. Note that the fast component is quickly obliterated by slowing of the capacity transient, which probably explains why this component has not yet, to our knowledge, been reported in squid axon.

Time Constant Versus Voltage and Charge Versus Voltage Data for the Components of Inactivated Gating Current. Families of gating currents like those in Fig. 2 were fitted to a sum of two or three exponentials. At V_p in the range of −100 mV to −60 mV the recovery time constant was constrained to the value obtained from a separate run on the same fiber using a long (20 ms) sampling window. The results of all fits are summarized in Fig. 3: Fig. 3*A* shows (on a semilogarithmic plot) the behavior of the time constants; Fig. 3*B* gives the charge–voltage (*Q–V*) relationships for the various components for different pulse protocols. The superimposed smooth curves were calculated from kinetic models presented in the *Discussion*. Note that most of the different fitted time constants at each V_p differ from each other by about an order of magnitude or greater; this emphasizes that the multiexponential fit was robust, the components being well-separated.

Each of the filled triangles at the top of Fig. 3*A* represents the mean (n = 2–9) of time constants from single exponential fits to the slowest ("recovery") component of each gating current recorded at that potential. For comparison, the open triangles plot the time constants for recovery of Na current at each potential, as measured in one fiber with a double-pulse paradigm (13). The remaining symbols in Fig. 3 denote individual double-exponential fits to $I_{g,inact}$, obtained using the three different pulse protocols discussed above (see Fig. 3 legend). Note that the values of the time constants measured at a particular V_p are the same irrespective of the starting voltage (−70 mV, 0 mV, or 50 mV), as expected for a memoryless process. (The figure excludes fast time constants for the prepulse to 50 mV and $V_p \geq -40$ mV because these gating currents were very small and sensitive to residual instrumentation asymmetries.) The fast time constants in Fig. 3*A* may be distorted by the slow tail in the capacity transient. On the other hand, the *Q–V* plot for the fast component (Fig. 3*Bd*) is not affected by slowness of the voltage clamp, provided that charge is integrated for long enough that the membrane potential has, indeed, settled to V_p. The fast *Q–V* curve is seen to saturate over a physiolog-

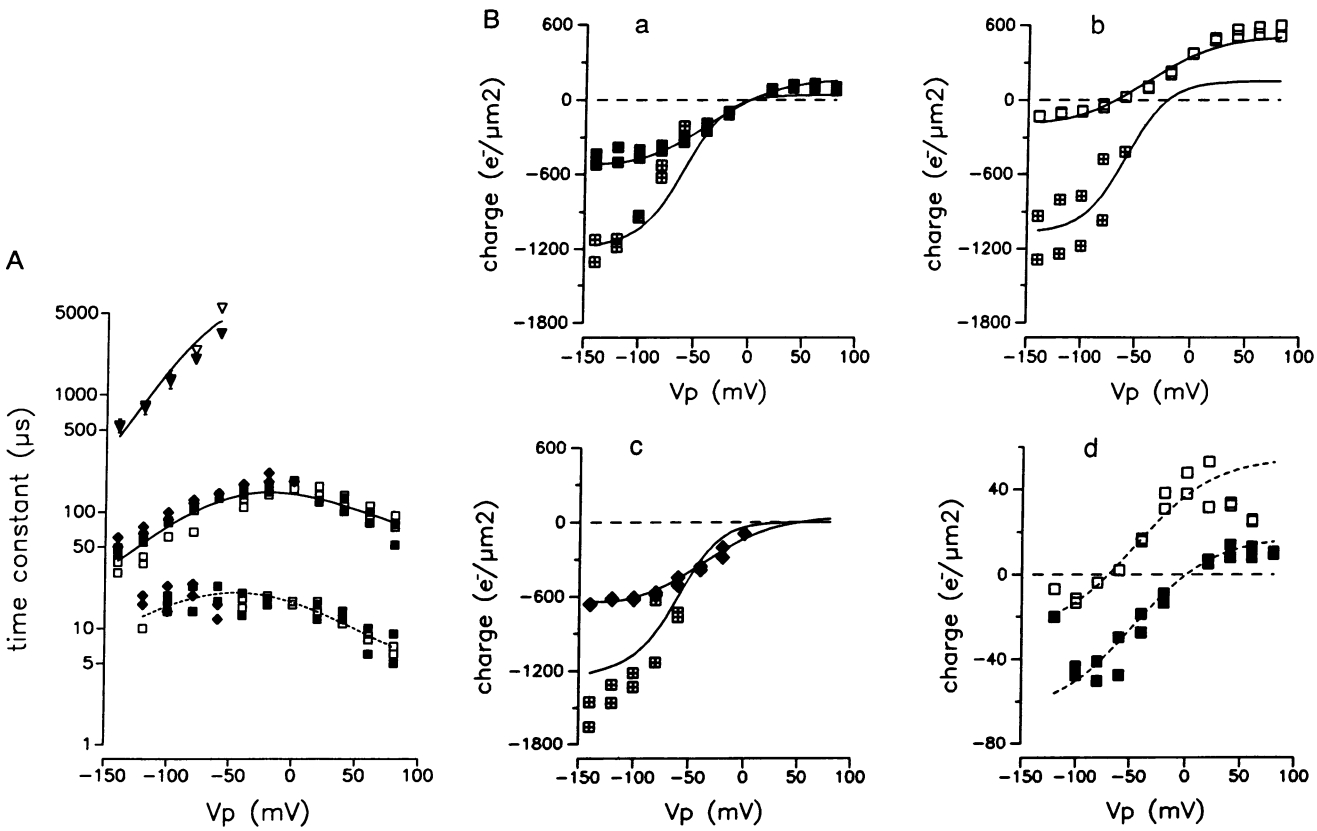

FIG. 3. Time constant versus voltage test membrane potential (V_p) and charge versus voltage data obtained from fits to gating currents like those shown in Fig. 2. (*A*) Collected time constants, showing the three widely spaced components observed. ■, Pulse paradigm of Fig. 2*A*; □, paradigm of Fig. 2*B*; ◆, paradigm of Fig. 2*C*; ▼, mean of two to nine measurements of the slowest (recovery) component, error bars on first three points being ± SEM; ▽, time constants for recovery of Na current measured in a separate experiment. (*B*) Charge [in electrons$^-$ (e^-) per μm^2] carried by each component for the various pulse paradigms. (*Ba–c*) *Q–V* plots for the recovery component (⊞) and $I_{g,inact}$ (slow), for paradigms *A–C*, respectively (same symbol convention as in *A*). (*Bd*) *Q–V* plots for $I_{g,inact}$ (fast) for paradigm *A* (■) and *B* (□). Broken curves were calculated from a two-state scheme with $a_{12} = 47\ ms^{-1}$, $a_{21} = 13\ ms^{-1}$, $q = 0.75\ e$, $n = 0.5$. Continuous curves were calculated from the three-state scheme in the text with $a_{R,I1} = 0.2\ ms^{-1}$, $a_{I1,R} = 0.02\ ms^{-1}$, $q_{R,I1} = 1\ e$, $n_{R,I1} = 0.15$, $a_{I1,I2} = 5.5\ ms^{-1}$, $a_{I2,I1} = 1.5\ ms^{-1}$, $q_{I1,I2} = 0.8\ e$, $n_{I1,I2} = 0.33$, where subscript I = inactivated and subscript R = resting.

ical range (around −100 mV to 50 mV). This, together with the voltage-dependent time constant, suggests that the fast component is truly an "asymmetry current" associated with a membrane protein.

A Fast Component Is Also Observed in the "ON" Na Gating Current. If the fast component is an asymmetry current, it can arise either from transitions among inactivated states of the Na channel (in which case it would be present only under inactivated conditions) or else from gating transitions that occur irrespective of the inactivation state of the channel (in which case it could always be present, contained within the total gating current). Fig. 4 provides evidence for the latter; *A* and *B* show the gating current measured in the same fiber at a constant test potential (20 mV) from a range of starting potentials (−120 to −20 mV). However, in Fig. 4*B* an inactivating prepulse is used, yielding $I_{g,inact}$, whereas in Fig. 4*A* the prepulse is omitted, yielding the gating current arising from transitions along the activation pathway and into the inactivated state(s), $I_{g,ON}$. A fast component, similar to $I_{g,inact}$ (fast), is apparent in $I_{g,ON}$ for all starting potentials. Such a component was clearly seen in all fresh fibers and at all positive test potentials and disappeared as the capacity transient slowed, just as did the fast component of $I_{g,inact}$.

An attempt was made to fit exponentials to $I_{g,ON}$ at test potentials where its shape appears simple ($V_p < -40$ mV) to look for a component with the same kinetic characteristics as $I_{g,inact}$ (fast). However, several time constants appeared present, but these were not well separated as for $I_{g,inact}$, rendering the fits inconclusive.

DISCUSSION

This work was motivated by the idea that Na channel gating kinetics are more easily and rigorously studied by initially focusing on small subsets of the channel's accessible states. Here we have attempted to analyze only those states occupied by the channel when it is inactivated. The benefit of doing this is immediately seen by comparing $I_{g,ON}$ and $I_{g,inact}$ (Fig. 4). $I_{g,ON}$, which arises from all the activation steps plus steps leading to inactivation, has a delayed decay, and

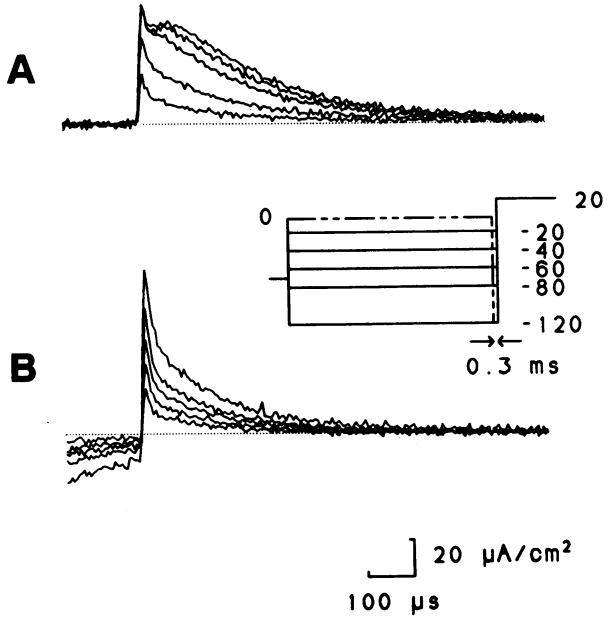

FIG. 4. A fast component is present in both $I_{g,ON}$ (*A*) and $I_{g,inact}$ (*B*). Note the spike that is always present at the beginning of $I_{g,ON}$ and which appears similar to that in $I_{g,inact}$. (*Inset*) Pulse paradigm: the inactivating prepulse, shown as a broken line, was absent to record $I_{g,ON}$ and present to record $I_{g,inact}$. Each trace is an average of four sweeps.

perhaps even a rising phase (after the initial spike) at some starting potentials. On the other hand, $I_{g,inact}$ is a simple biexponential process for all starting potentials and test pulses. Moreover, the two time constants describing $I_{g,inact}$ appear to depend only on the test potential and not on the initial conditions when these are varied from −70 mV to 50 mV (Fig. 3*A*).

It is important to note that, in general, the gating current generated by a multistate Markov model depends upon the rate constants and charge transfers between *all* the states (e.g., ref. 16). However, under certain conditions one can deal with a subset of the states in approximate isolation. If the rate of recovery from inactivated into resting states is very slow compared with the rates connecting the inactivated states, one can show that the relaxation time constants for the gating current originating in the inactivated states become independent of the rates connecting the resting states (e.g., ref. 16). However, some recovery does occur, and transitions among the resting states will give rise to gating current that may also have fast components, although their amplitudes may be small, depending on both the relative slowness of recovery and the relative amount of charge transfer among the resting and inactivated states. For present purposes it will be assumed that the conditions are such that gating current originating in the inactivated states predominates.

The problem is to find a simple kinetic model for the two components of $I_{g,inact}$ because this might shed light on their functional relationship. The following general scheme will be used in the discussion:

$$S_1 \underset{k_{21}}{\overset{k_{12}}{\rightleftharpoons}} S_2 \underset{k_{32}}{\overset{k_{23}}{\rightleftharpoons}} S_3$$
$$\leftarrow q_1 \rightarrow \leftarrow q_2 \rightarrow$$

Scheme I

with the indicated amount of charge flow q for each transition (see also ref. 5). This is the simplest model that could account for a biexponential process like $I_{g,inact}$. It is assumed that Eyring–Boltzmann kinetics are applicable (17) and that the transitions between the ith and jth states are governed by the voltage-dependent, time-independent rate constants

$$k_{ij} = a_{ij}\exp[nqV/kT], \quad [1]$$

and

$$k_{ji} = a_{ji}\exp[-(1-n)qV/kT]. \quad [2]$$

Here the a values are the values of the rates when the membrane voltage, V, is zero, q is the charge transfer when going from state i to j, and n is a number between 0 and 1 that gives the location of the peak of the energy barrier separating i and j, expressed as a fraction of the distance between those states. It can be shown that a plot of the logarithms of the gating current time constants predicted by Scheme I yields straight lines as $V \rightarrow \pm\infty$, with the slopes and intercepts of these lines giving values for the parameters a, n, and q in Eqs. 1 and 2. This enables one to decide quickly whether the model fits one's data.

The above approach was used to determine whether a model like Scheme I could fit the two components of $I_{g,inact}$. It was found that Scheme I could not fit $I_{g,inact}$, even allowing for the possibility that the time constant of $I_{g,inact}$ (fast) is distorted by the slow tail in the capacity transient: discrepancies with the model were too striking (e.g., inward currents measured where outward ones were predicted).

The next most complicated scheme is one with two independent two-step processes in parallel, which is equivalent to a single four-state scheme with some restrictions on the

interconnecting rates (4, 6). In this case, good fits to both components of $I_{g,inact}$ were obtained. For the fast component, the fitted parameters (see Fig. 3 legend) were used to calculate the broken lines in the τ–V and Q–V plots in Fig. 3 *A* and *Bd*. The agreement is satisfactory, except for the extremities of the Q–V curves. However, owing to the above-mentioned distortion of this component, this fit should be regarded with caution. A good fit to $I_{g,inact}$ (slow) could be obtained with q and n similar to those for the fast component, but the a values are an order of magnitude slower. The τ–V curve for $I_{g,inact}$ (slow) calculated from this model is very close to that shown in Fig. 3*A* (lower continuous curve); however, this curve was actually calculated from a slightly more general scheme for $I_{g,inact}$ (slow) that is discussed below.

The conclusion from the above is that the fast component of $I_{g,inact}$ can be modeled most readily by assuming that it is kinetically independent of $I_{g,inact}$ (slow). This assumption is compatible with the result of Fig. 4 that a fast component of gating current appears independent of the inactivation state of the Na gating system; however, more complex models that do couple the fast and slow components of $I_{g,inact}$ can certainly be conceived. An independent fast component could originate in functionally uncoupled conformational changes within the Na channel protein or in other membrane-spanning proteins, such as pumps (18), potassium channels (19, 20), or a distinct class of modified Na channels (2, 21).

The above two-state scheme for $I_{g,inact}$ (slow) might be extended by incorporating a third state to account for the recovery gating current ($I_{g,recov}$) that is seen at strongly hyperpolarized potentials (Fig. 2). Thus, the following variant of Scheme I was tested: $R \leftrightarrows I_1 \leftrightarrows I_2$. Here I_1 and I_2 represent inactivated states, and all the resting states are lumped under R, which is reasonable when transitions among R states are fast compared with the recovery step (16). We found that this did indeed provide a good fit to the τ–V and Q–V data for both $I_{g,inact}$ (slow) and $I_{g,recov}$ over a wide range of voltages and without any arbitrary renormalization, even in view of the fact that the data are pooled from different axons (smooth lines in Fig. 3 *A* and *Ba–c*; see legend for parameters). Thus, an inactivated squid Na channel seems able to switch rapidly between just two nonconducting states before eventually relaxing by means of a single step into other states from which reactivation may occur.

How might the above scheme be reconciled with general models of the squid Na channel, like those of Armstrong and Bezanilla (3) or Armstrong and Gilly (1)? The latter have inactivated states accessible both directly from the resting states and via the open configuration. However, at hyperpolarized potentials these models reduce to a special case in which recovery proceeds only by means of a single, voltage-dependent step directly to the resting states, to account for the observation that recovering channels do not conduct (22). Thus, our three-state scheme can be equated with certain parts of those more general schemes, at least under specific conditions. According to the fit to our data, the charge transfer in the recovery step is $\approx 1\ e$. This is the same as the value cited by Armstrong (4) for the corresponding process in his complete scheme. On the other hand, we find the charge flow between the two inactivated states to be $0.8\ e$, similar to the value of Stimers *et al.* (5) (1 *e*), but somewhat less than that given by Armstrong and Gilly (1) (2 *e*).

In summary, the experiments described here were designed to isolate and provide information about the inactivated states of the Na channel, as a prelude to integrating this process into a more complete model of the channel. We have also described a very fast component of gating current that is revealed under optimized recording conditions. These findings may be important for future structure–function studies of the Na channel.

We thank the Director and staff of the Station Marine, Roscoff, for squid; Prof. R. D. Keynes for dissection and electrode construction; and Prof. B. Neumcke and Dr. C. F. Stevens for helpful suggestions. S. B. Cross provided technical assistance. This research was supported by the Swiss National Foundation, Grant 3.143-0.85, to N.G.G.

1. Armstrong, C. M. & Gilly, W. F. (1979) *J. Gen. Physiol.* **74,** 691–711.
2. Chandler, W. K. & Meves, H. (1970) *J. Physiol. (London)* **211,** 653–678.
3. Armstrong, C. M. & Bezanilla, F. (1977) *J. Gen. Physiol.* **70,** 567–590.
4. Armstrong, C. M. (1981) *Physiol. Rev.* **61,** 644–683.
5. Stimers, J. R., Bezanilla, F. & Taylor, R. E. (1985) *J. Gen. Physiol.* **85,** 65–82.
6. Keynes, R. D. (1990) *Proc. R. Soc. London Ser. B.* **240,** 425–432.
7. Greeff, N. G., Keynes, R. D. & Van Helden, D. F. (1982) *Proc. R. Soc. London Ser. B.* **215,** 375–389.
8. Bekkers, J. M., Greeff, N. G., Keynes, R. D. & Neumcke, B. (1984) *J. Physiol. (London)* **352,** 653–668.
9. Forster, I. C. & Greeff, N. G. (1990) *J. Neurosci. Methods* **33,** 185–205.
10. Greeff, N. G., Benoit, C. & Sandri, C. (1990) *Biophys. J.* **57,** 129a (abstr.).
11. Greeff, N. G. (1986) in *Ion Channels in Neural Membranes*, eds. Ritchie, J. M., Keynes, R. D. & Bolis, L. (Liss, New York), pp. 53–59.
12. Stimers, J. R., Bezanilla, F. & Taylor, R. E. (1987) *J. Gen. Physiol.* **89,** 521–540.
13. Bezanilla, F. & Armstrong, C. M. (1977) *J. Gen. Physiol.* **70,** 549–566.
14. Forster, I. C., Greeff, N. G. & Keynes, R. D. (1988) *Experientia* **44,** A72 (abstr.).
15. Alicata, D. A., Rayner, M. D. & Starkus, J. G. (1989) *Biophys. J.* **55,** 347–353.
16. Colquhoun, D. & Hawkes, A. G. (1977) *Proc. R. Soc. London Ser. B.* **199,** 231–262.
17. Bezanilla, F. (1985) *J. Membr. Biol.* **88,** 97–111.
18. Boron, W. F., Hogan, E. & Russell, J. M. (1988) *Nature (London)* **332,** 262–265.
19. Gilly, W. F. & Armstrong, C. M. (1980) *Biophys. J.* **29,** 485–492.
20. White, M. W. & Bezanilla, F. (1985) *J. Gen. Physiol.* **85,** 539–554.
21. Matteson, D. R. & Armstrong, C. M. (1982) *J. Gen. Physiol.* **79,** 739–758.
22. Armstrong, C. M. & Croop, R. S. (1982) *J. Gen. Physiol.* **80,** 641–662.